Enhanced electronic conductivity in Si-substituted calcium aluminate

Mariana I. Bertoni and Thomas O. Mason
Department of Materials Science and Engineering, Northwestern University, Evanston, Illinois 60208, USA

Julia E. Medvedeva[a)]
Department of Physics, University of Missouri-Rolla, Rolla, Missouri 65409, USA

Yongqiang Wang
Ion Beam Materials Laboratory, Los Alamos National Laboratory, Los Alamos, New Mexico 87545, USA

Arthur J. Freeman
Department of Physics and Astronomy, Northwestern University, Evanston, Illinois 60208, USA

Kenneth R. Poeppelmeier
Department of Chemistry, Northwestern University, Evanston, Illinois 60208, USA

(Received 24 May 2007; accepted 28 September 2007; published online 4 December 2007)

Improved conductivity has been achieved by controllable substitution of an ultraviolet electronic conductor. The transparent conducting oxide system, H-doped $Ca_{12}Al_{(14-x)}Si_xO_{(33+x/2)}$ with $x=0-4$, exhibits a conductivity strongly dependent on the substitution level. Four-point direct current conductivity increases with x from 0.15 to 0.61 S/cm at room temperature. The observed conductivity behavior is consistent with the predictions of our first principles density functional calculations for the Si-substituted system with $x=0$, 2, and 4. Furthermore, the Seebeck coefficient is composition dependent suggesting the existence of an activated mobility associated with small polaron conduction. © *2007 American Institute of Physics*. [DOI: 10.1063/1.2817605]

I. INTRODUCTION

Transparent conducting oxides (TCOs) are materials that exhibit high transparency in the visible range of the electromagnetic spectrum as well as high electrical conductivity. Thin films of these materials find applications as transparent electrodes in a wide range of devices including flat-panel displays, electrochromic windows, photovoltaic systems, deicers, and emerging applications such as flexible and invisible electronics.[1–5] The common way to achieve the two mutually exclusive characteristics of transparency and conductivity is by degenerately doping a wide band gap oxide, pushing the Fermi level into the conduction band, but this approach is not applicable to oxides of the main group metals. Based on the need for inexpensive and environmentally benign TCO alternatives, new processes are being studied to render these oxides conducting. In 2002, the well-known insulating oxide $12CaO \cdot 7Al_2O_3$, widely used in high-alumina cements, was discovered to be rendered conductive by hydrogen doping and subsequent ultraviolet light (UV) irradiation. The system, also referred to as $Ca_{12}Al_{14}O_{33}$ or mayenite, has a cubic crystal lattice with a lattice parameter of 1.199 nm and space group $I\bar{4}3d$.[6] It possesses a cage structure with two formula units (12 cages) per unit cell and its empirical formula may be written as $[Ca_{24}Al_{28}O_{64}]^{+4}+2O^{-2}$, where the former denotes the lattice framework and the latter are the free oxygen ions that provide charge neutrality to the positively charged framework (Fig. 1).

As was proposed in the original report, $Ca_{12}Al_{14}O_{33}$ incorporates hydrogen at elevated temperatures through the following chemical reaction:[7]

$$O^{-2} + H_2 \rightarrow OH^- + H^-. \quad (1)$$

After hydrogen incorporation, the unit cell contains two cages occupied by OH^-, another two occupied by H^- and the remaining eight cages of the unit cell are empty. Hydrogen annealing results in no apparent change in the optical and electrical properties of the material. However, upon irradiation two optical absorption bands are induced, giving rise to a persistent color change from white to green, together with a dramatic conductivity increase from 10^{-10} to 0.3 S/cm at room temperature. The first report suggested that the carriers originated from ultraviolet irradiation according to

$$H^- + \text{energy} \rightarrow H^0 + e^- + \text{phonon}. \quad (2)$$

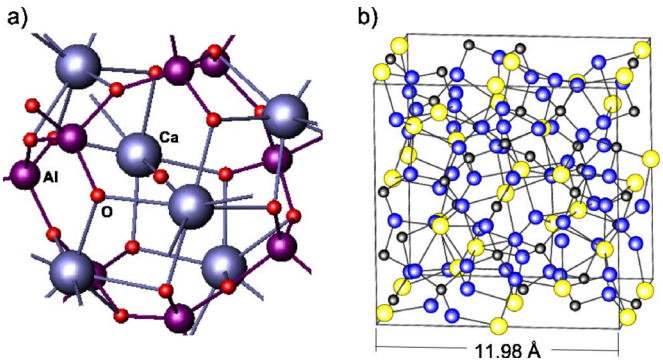

FIG. 1. (Color online) (a) A single cage of $Ca_{12}Al_{14}O_{33}$. (b) Unit cell of $Ca_{12}Al_{14}O_{33}$ containing 12 cages.

[a)]Author to whom correspondence should be addressed. Electronic mail: juliaem@umr.edu.

Even though all of the existent reports seem to agree about the creation of carriers due to UV irradiation, the stability of the H^0 and the precise reaction is still a topic under study.[8,9]

Our previous investigations revealed the hopping nature of the photoexcited electron in H-doped UV-irradiated $Ca_{12}Al_{14}O_{33}$.[10–12] The knowledge of the transport mechanism predicted a strong dependence of the light-induced conductivity on the specific atoms participating in the hopping as well as on their spatial arrangement, i.e., the hopping path. This previous work showed the possibility of tuning the conductivity by proper isovalent substitution of Mg for Ca, where increasing amounts of magnesium led to a decrease in conductivity.[12]

In this work, the conduction mechanism of Si-substituted mayenite was studied both experimentally and theoretically, exploring the idea that the aliovalent substitution of Al^{3+} by Si^{4+} will force the unit cell to accommodate more free oxygen ions O^{-2} to balance the framework, allowing more hydrogen ions to be incorporated into the sample and, hence, more electrons to be released after UV light irradiation. Equations for the hydrogen treatment and UV light activation will now be dependent on the substitution level.

Free oxygen per unit cell

$$2[Ca_{12}Al_{14-x}Si_xO_{33+x/2}] \rightleftharpoons 2[Ca_{12}Al_{14-x}Si_xO_{32}]^{(x+2)-} + (x+2)O^{2-}. \quad (3)$$

Hydrogen treatment

$$(x+2)O^{-2} + (x+2)H_2 \rightarrow (x+2)OH^- + (x+2)H^-. \quad (4)$$

UV-irradiation

$$(x+2)H^- + \text{energy} \rightarrow (x+2)H^0 + (x+2)e^- + \text{phonon}. \quad (5)$$

In addition, we present a small polaron mechanism that is consistent with the electronic conduction in this system and discuss the conductivity behavior observed for $Ca_{12}Al_{(14-x)}Si_xO_{(33+x/2)}$ based on the results and predictions of our first-principles band structure calculations.

II. METHODOLOGIES

A. Experimental

Samples of Si-substituted $12CaO \cdot 7Al_2O_3$ were obtained by hydrothermal synthesis. It was shown by Fujita *et al.* that hydrothermal synthesis of the metastable Si-substituted mayenite can be achieved through a garnet precursor.[13,14] The hydrous component of the garnet, named grossular, $Ca_3Al_2(SiO_4)_3$, is the hydrogarnet precursor for this synthesis where (OH^-) groups substitute some (SiO_4)-tetrahedra.[15] High purity $Ca(OH)_2$, amorphous-SiO_2 and γ-Al_2O_3 (>99.99%, Alfa Aesar) were mixed in an agate mortar in the presence of acetone. Once the acetone was evaporated, stoichiometric amounts of the starting powders were placed in a 125 mL polytetrafluoroethylene or Teflon (PTFE) (Teflon)-lined autoclave (Parr Inst. Co) with 12 mL of H_2O per gram of powder. The autoclave was then sealed and ramped to 200 °C in 2 h, the system was held at that temperature for 13–15 h, and then cooled down to room temperature. The reaction under these conditions is

$$3Ca(OH)_2 + \gamma - Al_2O_3 + (3-y)SiO_2 \xrightarrow{H_2O} Ca_3Al_2(SiO_4)_{(3-y)}(OH)_{4y} \quad (6)$$

for $y=2.8$, 2.6, 2.4, and 2.2. Note that the stability of the hydrogarnet decreases with increasing silica content in the bulk composition and with increasing reaction time, so it is important to keep these variables well controlled. The product of the hydrothermal synthesis was filtered and rinsed with water and ethyl alcohol to prevent carbonization of the material.[16] Subsequently, it was dried out overnight at 120 °C and x rayed. Once the phase purity was confirmed, the hydrogarnet precursor ($y=2.8$, 2.6, 2.4, and 2.2) was calcined at 800 °C for 15–24 h to obtain the desired phase of $Ca_{12}Al_{(14-x)}Si_xO_{(33+x/2)}$ ($x=1$, 2, 3, and 4),

$$\left(7-\frac{x}{2}\right)Ca_3Al_2(SiO_4)_{(3-y)}(OH)_{4y} \rightarrow Ca_{12}Al_{14-x}Si_xO_{33+x/2} + \left(9-\frac{3x}{2}\right)CaO + (14y-xy)H_2O + \left[21-7y-\frac{x}{2}(1+y)\right]SiO_2. \quad (7)$$

As noted in previous reports, a small weight percent of lime is a by-product of the reaction. The $Ca_{12}Al_{(14-x)}Si_xO_{(33+x/2)}$ phase is not stable enough to withstand the complete chemical removal of the CaO phase, so the measurements were performed with small amounts of residual CaO (<5% weight, from Rietveld refinements). Pellets of 11.6 mm diameter×2–3 mm thickness were pressed at 180 MPa and heated up in air at 800 °C for 2–3 days.

The phase purity of the samples was confirmed by powder x-ray diffraction using Cu $K\alpha$ radiation (Rigaku, MA). The tube was operated at 40 kV and 20 mA and a nickel filter was used to remove the Cu $K\beta$ contribution from the diffraction pattern. For routine phase analysis, powders were scanned between 10° and 80° in 2θ with a step size of 0.05° and a dwell time of 1 s.

Hydrogen treatment at elevated temperatures as implemented in previous reports[12,17] was ruled out owing to the instability of the Si-substituted samples. Instead, ion implantation was performed at Los Alamos National Laboratory. The working parameters found for these samples were 57.5 keV of H^+ beam to a fluence of 1×10^{18} atoms/cm^2 at 300 °C, after which a colored layer is induced on the surface of the samples.[18] It should be noted that a first implantation attempt was carried out at 600 °C but the $Ca_{12}Al_{(14-x)}Si_xO_{(33+x/2)}$ phase started to decompose.

A thermogravimetric analysis (TGA) was performed on the hydrogarnet precursor $Ca_3Al_2(SiO_4)_{(3-y)}(OH)_{4y}$ to study the loss of H_2O in the transformation to $Ca_{12}Al_{(14-x)}Si_xO_{(33+x/2)}$ as related to the Si-substitution level. Measurements were made on a TA Instruments TGA 2950 thermogravimetric analyzer. The heating profile was a linear

ramp from room temperature to 800 °C at 5 °C/min; the sample was held isothermally at 800 °C for 12 h and then allowed to cool down.

Conductivity measurements between room temperature and 500 °C were taken using the Van der Pauw technique, where a four-point spring-loaded probe touches the sample in four different points close to the edges.[19] The resistance, $R_{AB,CD}$, is defined as the potential difference $(V_D - V_C)$ between the contacts D and C per unit current flowing through the contacts A and B. Similarly a resistance $R_{BC,DA}$ can be defined and the following relation holds for a specimen of arbitrary shape:

$$\exp\left(-\pi R_{AB,CD}\frac{d}{\rho}\right) + \exp\left(-\pi R_{BC,DA}\frac{d}{\rho}\right) = 1, \tag{8}$$

where ρ is the resistivity of the material and d is the thickness of the UV-activated slab. In every case, corrections were made for layer thickness and sample diameter. It should be mentioned that corrections for porosity were not performed on any of the UV irradiated mayenite samples owing to the uncertainty in the properties of the irradiated layer.

Room temperature thermopower data were collected on bar-shaped samples cut from the pellets with an Isomet slow speed saw (Buehler, Ltd., IL). The bars of approximately 10 mm×3 mm×3 mm were sandwiched lengthwise between two gold foil contacts. The bars were painted on the contact faces with a silver colloidal suspension to improve the electrical and thermal contact between the small UV-activated layer and the two gold electrodes. One gold contact was in thermal equilibrium with a 23 W heating element and the other was in thermal equilibrium with a cylindrical steel slug that rested on an insulating ceramic brick. A type S (Pt-Pt/10% Rh) thermocouple bead was welded to both gold contacts. A thermal gradient was created by switching on the heating element and allowing it to reach 100 °C, at which point, the heating element was switched off, letting the system relax thermally. The temperature difference (ΔT) and the voltage difference (ΔV) were measured at regular intervals (3 s) using a programmable scanner (Keithley 705, Cleveland, OH) and a digital multimeter (Keithley 195A, Cleveland, OH) connected through an IEEE port to a personal computer. Thermopower was calculated by fitting the temperature and voltage gradient data with a least-squares fit as the sample approached equilibrium using the concept presented by Hong *et al.*,[20]

$$Q = -\lim_{\Delta T \to 0}\frac{\Delta V}{\Delta T}. \tag{9}$$

A correction for the contribution of the Pt thermocouple to the overall thermopower was made using the polynomial fit of Hwang,[21]

$$Q_{actual} = Q_{measured} + Q_{Pt}. \tag{10}$$

The optical properties of the bulk specimens were estimated from diffuse reflectance measurements, since thin films of these materials were unavailable for direct transmission data. The spectra for the specimens were collected on a Cary 500 UV-visible-near-infrared spectrophotometer (Varian Instruments, Inc., Palo Alto, CA) using a diffuse reflectance accessory between 250 and 800 nm with a lead sulfide detector. The accessory has the ability to collect most reflected radiation, remove any directional preferences, and present an integrated signal to the detector. In diffuse reflectance, the nonspecular component of reflection is measured relative to a standard (pressed PTFE powder) using an integrating sphere. The spectra are analogous to transmission spectra on films and allow determination of the absorption edge onset.

B. Theoretical methods

First-principles density functional electronic band structure calculations for pure and H-doped $Ca_{12}Al_{(14-x)}Si_xO_{(33+x/2)}$ ($x=0$, 2, and 4) were performed using both the full-potential linearized augmented plane wave[22] (FLAPW) and linear muffin-tin orbital[23] methods within the local density approximation. The latter was used to model the UV-irradiated mayenite. To do this, we calculated a system where the electron(s) excited off the encaged hydrogen ion(s) H^- is(are) transferred to the states of neighboring Ca atoms which form the conduction band and are located ~5 eV above the states of the encaged hydrogen. The transition energy corresponds to the observed maximum efficiency of the UV activation.[7,10] (We note here that the modeled UV-irradiated systems stay neutral.) All calculations were performed for the cell of mayenite with one formula unit (i.e., 59 atoms per cell which combine into six cages) with periodic boundary conditions. As expected, upon structural relaxations performed via total energy and atomic force minimization within the FLAPW method, the encaged oxygen moves closer to Si^{4+} by 0.34 Å, as compared to the distance between the O^{2-} ion and its nearest Al^{3+} neighbor in the unsubstituted mayenite. The mutual spatial arrangement of the Si atoms and the encaged defects, O^{2-}, OH^-, and H^-, was investigated via total energy comparisons. We found that in H-doped UV-irradiated $Ca_{12}Al_{(14-x)}Si_xO_{(33+x/2)}$ for $x=0$, the most energetically favorable configuration corresponds to the shortest hopping path.[10,24,25] When the number of the encaged defects is doubled, $x=2$, or tripled, $x=4$ (in the later case, all cages are occupied by OH^- and H^-), the lowest total energy configuration is the one with the largest band splitting at the Fermi level. The splitting leads to the appearance of a partially filled Coulomb gap—a distinctive feature of the observed variable range hopping behavior of the conductivity.

III. RESULTS AND DISCUSSION

Figure 2 shows results of the thermogravimetric studies conducted on powder samples of as-prepared $Ca_3Al_2(SiO_4)_{(3-y)}(OH)_{4y}$. The experimental values are in very good agreement with the calculated values confirming the substitution levels and their correspondence to the previously calculated lattice parameters. Table I compares the experimental loss to that calculated on the basis of Eq. (7).

Figure 3 shows the temperature dependence of the conductivity for proton-implanted/UV-irradiated Si-substituted mayenite between room temperature and ~100 °C. The results show a thermally activated dependence of the conduc-

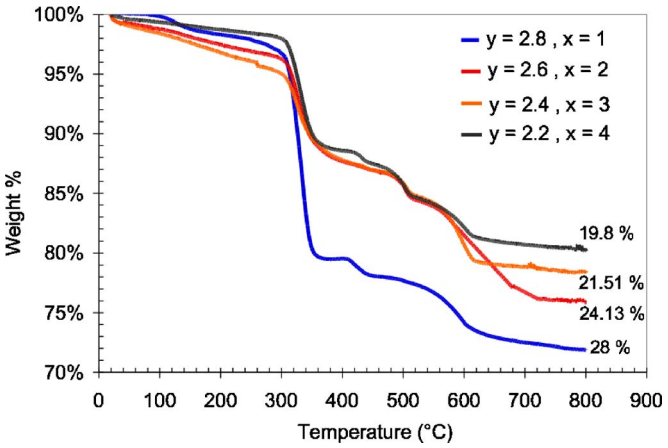

FIG. 2. (Color online) Thermogravimetric analysis of $Ca_3Al_2(SiO_4)_{(3-y)} \times (OH)_{4y}$ powders heated to 800 °C in air.

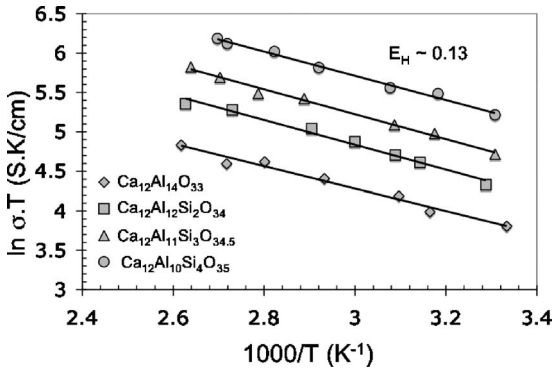

FIG. 3. Temperature dependence of the conductivity for UV-irradiated proton implanted $Ca_{12}Al_{(14-x)}Si_xO_{(33+x/2)}$ $(x=2,3,4)$ obtained by hydrothermal synthesis and UV-irradiated proton implanted $Ca_{12}Al_{14}O_{33}$ obtained by solid state.

tivity and an increase in the values with the substitution level consistent with the idea that the higher the substitution level, the more hydrogen is incorporated into the sample and the more electrons are released after UV light irradiation. Although the systematic error is on the order of 5% due to the uncertainty of geometric factors, the random uncertainty is on the order of the symbol size or less.

At room temperature, the conductivity rises from 0.15 S/cm for the nonsubstituted specimen to 0.61 S/cm for the maximum substitution, $Ca_{12}Al_{10}Si_4O_{35}$. The value for the nonsubstituted specimen is at the lower end of previously reported values of conductivity,[7,12] which suggests small amounts of hydrogen are incorporated into these samples, most probably this is due to the low temperatures used during hydrogen implantation (300 °C). However, the present work is concerned with the relative changes between samples caused by the Si substitution. Within experimental error, the slopes in Fig. 3 are essentially identical, giving a hopping energy (E_H) of 0.13 eV.

The thermoelectric coefficient was measured at room temperature and at 90 °C for the different substitution levels. Figure 4 shows that the Seebeck coefficient is roughly temperature independent in the range of 25–100 °C and only slightly dependent on substitution level, consistent with the model proposed in Eq. (5). Table II summarizes the thermoelectric results obtained for the $Ca_{12}Al_{(14-x)}Si_xO_{(33+x/2)}$ phase at room temperature, where the negative sign of the Seebeck coefficient indicates that the carriers are electrons (*n* type). The fact that the conductivity is thermally activated while the Seebeck coefficient is roughly temperature independent establishes the existence of an activated mobility and suggests that the electronic transport mechanism is by small polaron hopping, similar to the previously reported systems, $Ca_{12}Al_{14}O_{33}$ and $Ca_{(12-x)}Mg_xAl_{14}O_{33}$.[10,12]

TABLE I. Expected weight loss from Eq. (7) vs experimental weight loss from TGA measurements.

Substitution level (x)	Calculated weight loss (%)	Experimental weight loss (%)
1	26.32	28
2	24.13	24.13
3	22.1	21.51
4	19.93	19.8

A polaron is a pseudoparticle used to describe the carrier and its associated lattice distortion. When the local lattice distortion induced by the moving electron extends over distances smaller than the lattice constant, we are in the small polaron regime. Transport in this kind of system happens by thermally activated hopping in which, contrary to all other conduction mechanisms, lattice vibrations do not reduce the electron mobility but rather enhance it.[26] Large effective masses and narrow bands are characteristics of this mechanism. The mobilities associated with this mechanism are typically lower than 1 $cm^2/V\,s$, and their low to intermediate conductivities are often accompanied by very small (sometimes negligible) activation energies. The usual means for demonstrating small polaron behavior is by showing an activated mobility, which is generally straightforward when the conductivity is thermally activated and the thermopower is not, or when the conductivity has a significantly larger activation energy compared to that of the thermopower.

The thermopower or Seebeck coefficient, Q, is a useful estimate of the carrier content and for a small polaron mechanism Q can be written as

$$Q = \pm \frac{k}{e}\left[\ln\frac{2(1-c)}{c}\right], \tag{11}$$

where k/e is 86.14 $\mu V/K$, c is the fraction of conducting ions of higher valence; the factor 2 accounts for the spin

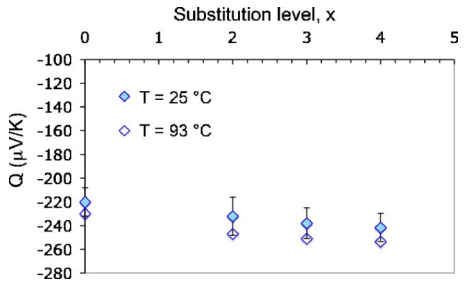

FIG. 4. (Color online) Thermopower for UV-irradiated proton implanted $Ca_{12}Al_{(14-x)}Si_xO_{(33+x/2)}$ $(x=2,3,4)$ obtained by hydrothermal synthesis and UV-irradiated proton implanted $Ca_{12}Al_{14}O_{33}$ obtained by solid state.

TABLE II. Thermoelectrical properties of UV-irradiated proton implanted $Ca_{12}Al_{14}O_{33}$ and $Ca_{12}Al_{(14-x)}Si_xO_{(33+x/2)}$ $(x=2,3,4)$.

Substitution level (x)	Conductivity room temperature (S/cm)	Thermopower room temperature (μV/K)	Fraction of occupied sites (c)
0	0.15	−220±12	0.134
2	0.25	−232±16	0.119
3	0.37	−238±13	0.112
4	0.61	−241±12	0.108

degeneracy, and the sign is determined by the nature of the polaron.[27] Based on the experimental result of the thermopower shown in Fig. 4, the fraction of conducting species decreases with increasing substitution level, which at first glance seems to be opposite to our predictions. The calculated values of the fraction of occupied sites (c) are also listed in Table II.

The small polaron hopping conductivity is given by

$$\sigma = \frac{\sigma_0}{T} \exp\left(\frac{-E_H}{kT}\right), \tag{12}$$

where E_H is the hopping energy and σ_0 is the pre-exponential factor defined as

$$\sigma_0 = \frac{gcN(1-c)e^2a^2\nu}{k}. \tag{13}$$

Here g is a geometric factor, c is the fraction of sites occupied by carriers, ν is the optical mode phonon frequency, a is the hopping distance from site to site, and N is the total number of available sites related to the total number of carriers by $n=Ne$.[27] As mentioned before, the activation energy values are the same for the different substitution levels and compare favorably with typical values of small polaron behavior.[28–30] On the other hand, the values of the pre-exponential factor are significantly different, showing an increase with higher substitution levels (see Fig. 3). Assuming that the geometric factor (g), the vibrational frequency (ν), and the jump distance (a) remain almost constant with substitution level, it is clear that the number of available sites N must increase in proportion to the Si substitution level, which is consistent with the equations introduced previously [Eqs. (4) and (5)].

In order to relate the thermopower data to the conductivity, the product $c(1-c)$ and the pre-exponential values (σ_0) taken from the intercepts of Fig. 3 were plotted versus the substitution level, x. Figure 5 shows that the factor $c(1-c)$ follows the opposite trend as the pre-exponential value (σ_0) with x and that the difference between the trends increases with substitution level. When analyzing the variables in the pre-exponential term given by Eq. (13) it is clear that not only the number of carriers per unit cell, but also the number of hopping centers increases with x. Significantly, the total number of available sites for hopping increases faster with the Si content in $Ca_{12}Al_{(14-x)}Si_xO_{(33+x/2)}$ than the number of carriers. The latter observation is in accord with results of our electronic band structure calculations reported below: we find that not all extra electrons participate in hopping. In addition, we believe that the presence of other oxygen radicals, e.g., O_2^{-2} and O_2^- inside the cages of the silicon-substituted samples may result in the appearance of additional hopping centers as well as carrier donors. Investigations of the radical formation and the interaction between the encaged oxygenous and hydrogenous species are beyond the scope of the present work.

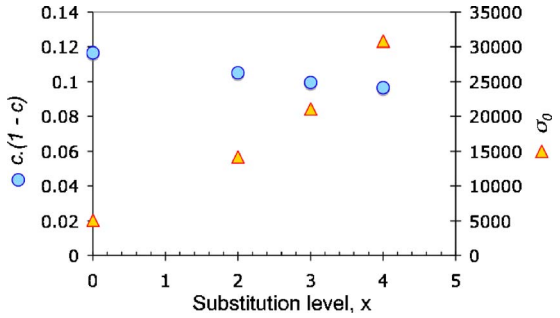

FIG. 5. (Color online) Pre-exponential values and $c(1-c)$ vs substitution level $Ca_{12}Al_{(14-x)}Si_xO_{(33+x/2)}$ $(x=0,2,3,4)$.

Finally, diffuse reflectance data for the proton-implanted/UV-irradiated $Ca_{12}Al_{10}Si_4O_{35}$ phase are shown in Fig. 6, compared with the $Ca_{12}Al_{14}O_{33}$ system that underwent the same treatment. Both systems are highly transparent before activation, showing 95% transmission in the visible spectrum, and band gaps of 4.43 and 4.76 eV, for the $Ca_{12}Al_{14}O_{33}$ and $Ca_{12}Al_{10}Si_4O_{35}$, respectively. After activation, transmission decreases to 65% for pure mayenite and to 53% for the Si-substituted specimens, which is consistent with the higher carrier content of the latter sample.

IV. ELECTRONIC BAND STRUCTURE CALCULATIONS

The important feature of the electronic band structure of nanoporous $Ca_{12}Al_{14}O_{33}$ is the presence of a so-called cage conduction band[31] (or cavity conduction band[32]) located close to the framework conduction band formed from the Ca d states. In mayenite, the cage conduction band consists of five bands [Fig. 7(a)] that corresponds to the five empty cages out of the total six cages in the unit cell. One cage is occupied by an O^{2-} ion, resulting in a splitting of one band from the cage conduction band and its shift to a lower energy; a triply degenerate band that corresponds to p_x, p_y, and p_z orbitals is fully occupied and located below the Fermi level [Fig. 7(a)]. Upon substitution with Si, the cage conduction band, which now consists of four and three empty bands

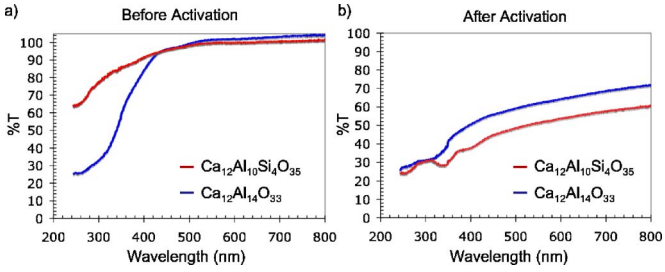

FIG. 6. (Color online) Diffuse reflectance of UV-irradiated proton implanted $Ca_{12}Al_{10}Si_4O_{35}$ compared to $Ca_{12}Al_{14}O_{33}$.

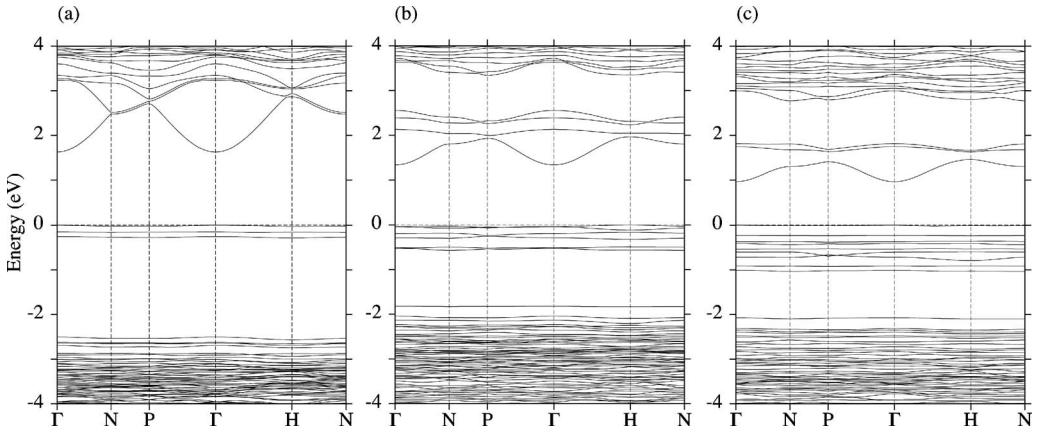

FIG. 7. Electronic band structure for $Ca_{12}Al_{(14-x)}Si_xO_{(33+x/2)}$ with $x=0$ (a), $x=2$ (b), and $x=4$ (c).

for $x=2$ and 4, respectively, Figs. 7(b) and 7(c), splits from the framework conduction band by about 1 eV, as obtained in local density approximation calculations.

Significantly, it was found that the forbidden gap between the states of the encaged oxygen ions and the cage conduction band decreases from 1.6 eV for $x=0$ to 1.3 and 0.9 eV for $x=2$ and 4, respectively. This results in a lower dispersion of the bottom of the cage conduction band with higher Si content. (We note here that the optical band gap is from the top of the valence band while the energy levels associated with the O^{2-} ions are "defect" bands.)

The incorporation of hydrogen, which occurs according to the chemical reaction of Eq. (4), results in the appearance of new bands: filled σ, nonbonding π, and unoccupied σ' bands (these correspond to the OH^- complex) and a fully occupied band below the Fermi level formed from the 1*s* states of the encaged H^-.[10] For $x=2$ or 4, the number of bands increases accordingly to two or three occupied bands for the two or three encaged H^- ions, and two or three empty σ' bands for two or three OH^- complexes, respectively.

Figure 8 shows the electronic band structure of H-doped and UV-activated $Ca_{12}Al_{(14-x)}Si_xO_{(33+x/2)}$ systems. Similar to unsubstituted mayenite,[10] the UV irradiation of the Si-doped structures results in the appearance of a new hybrid band that crosses the Fermi level making the system conducting. For $x=0$, 2, and 4, the new band consists of two, four, and six bands, respectively (Fig. 8). This corresponds to the total number of the encaged defects, i.e., the hydrogen ions (bands below E_F) and the OH^- complexes (bands above E_F), in the unit cell.

An analysis of the atomic contributions to the band suggests that only the encaged defects and their nearest Ca atoms participate in the charge transport. The most energetically favorable spatial arrangement of the atoms which contribute to the density of states near E_F corresponds to the shortest hopping path. For unsubstituted mayenite ($x=0$), there is only one hopping path in the unit cell.[10,12] Strong Coulomb repulsion between the electrons that move along this narrow path leads to the appearance of a soft gap in the density of states at E_F. Upon Si substitution, the number of hopping centers (the encaged hydrogen ions, OH^- complexes and their nearest Ca neighbors) as well as the number of carriers (the electrons excited off the H^- ions or introduced by H^+ implantation) increases. As a result, the UV-released electrons have more freedom (Fig. 9) and the density of states at E_F increases (Fig. 8), leading to the observed increase in the conductivity compared to unsubstituted mayenite ($x=0$).

It is important to stress here that the enhanced conduc-

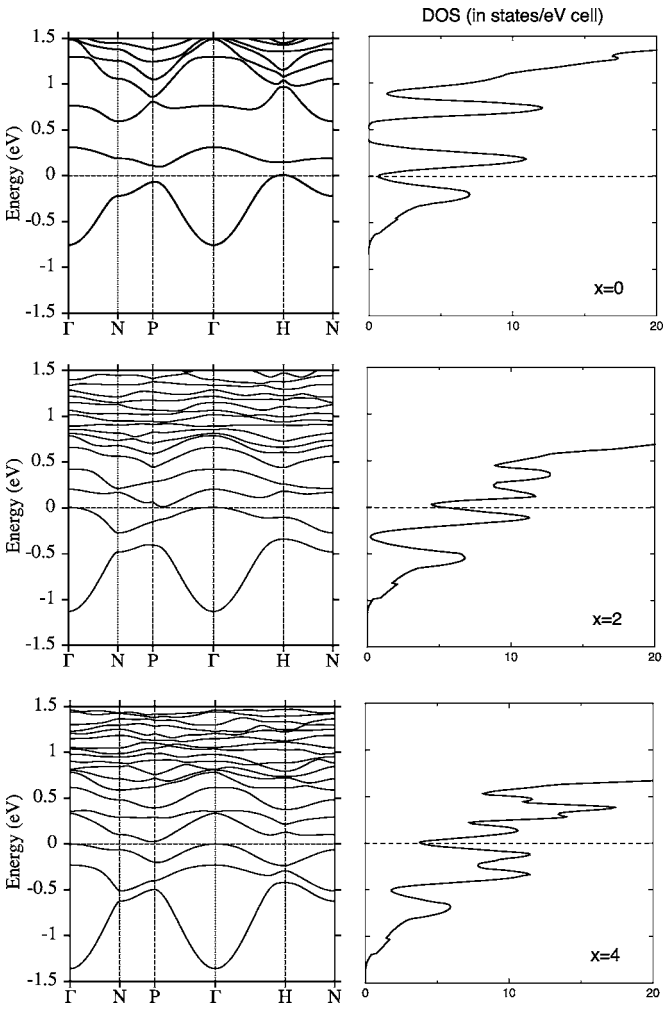

FIG. 8. Electronic band structure (left column) and density of states, in states/eV cell, (right column) for H-doped and UV-irradiated $Ca_{12}Al_{(14-x)}Si_xO_{(33+x/2)}$ with $x=0$ (top row), $x=2$ (middle row), and $x=4$ (bottom row).

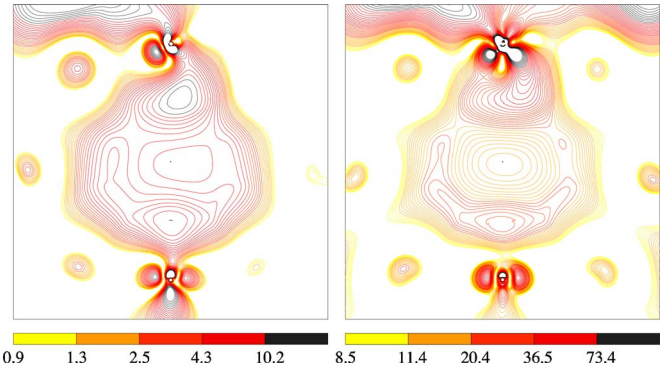

FIG. 9. (Color online) Contour map of the charge density distribution within a slice passing through the center of a cage with a hydrogen ion and its nearest Ca atoms for $Ca_{12}Al_{(14-x)}Si_xO_{(33+x/2)}$ with $x=0$ (left) and $x=4$ (right). The charge values are in 10^{-5} and 10^{-4} e/Å for $x=0$ and $x=4$, respectively.

tivity is primarily due to the increase in the number of sites available for hopping (that helps to overcome the strong Coulomb repulsion in the unsubstituted mayenite[10,24]) while the number of carriers increases more gradually with x. As seen from Fig. 8, the density of states becomes broader when x is increased: the width of the occupied part of the band (which consists of one, two, or three single bands), is found to be 0.75, 1.22, and 1.35 eV for $x=0$, 2, and 4, respectively. Therefore, some of the electrons have lower energy so that they become bound and do not hop. This finding is in excellent agreement with our observations based on the thermopower measurements discussed earlier.

V. CONCLUSIONS

Hydrothermal synthesis of the metastable phase of $Ca_{12}Al_{(14-x)}Si_xO_{(33+x/2)}$ and the subsequent H doping by ion implantation were achieved. Insulator-to-conductor conversion was observed similar to the cases of $Ca_{12}Al_{14}O_{33}$ and $Ca_{(12-x)}Mg_xAl_{14}O_{33}$. The electrical conductivity of the $Ca_{12}Al_{(14-x)}Si_xO_{(33+x/2)}$ system doubled or tripled the conductivity of nonsubstituted mayenite, with values of 0.25 S/cm for $x=2$ and 0.61 S/cm for $x=4$. The Seebeck coefficient shows no temperature dependence, but seems to be affected by the substitution level with a slight increase from -220 μV/K ($x=0$) to -240 μV/K ($x=4$). Similar to the unsubstituted mayenite system, the $Ca_{12}Al_{(14-x)}Si_xO_{(33+x/2)}$ phase appears to obey a small polaron conduction model with a similar hopping energy of 0.13 eV. From thermopower measurements, a decrease in the fraction of occupied sites is observed. At the same time, we find that an increase in the electron population is accompanied by an even higher increase in the number of hopping centers which explains the observed conductivity increase. Significantly, the results show a remarkable correlation with the theoretical predictions.

The spatial arrangement of the Si atoms and the various encaged defects which serve as hopping centers makes calculations of the probable hopping paths a complex task. Consequently, estimates of the carrier mobility and content are impossible. Optical properties are consistent with the electrical results, showing a decrease in transmission with the increase in Si content, concomitant with the increase in the carrier content.

Finally, although the experimental manipulation of this metastable phase makes any practical application extremely cumbersome, $Ca_{12}Al_{(14-x)}Si_xO_{(33+x/2)}$ exemplifies the origin of the electron conductivity in the mayenite-based systems.

ACKNOWLEDGMENTS

This work was supported by the MRSEC program of the National Science Foundation at Northwestern University (DMR-0076097), by the Department of Energy (DE-FG02-88ER45372), and by the University of Missouri Research Board.

[1] D. S. Ginley and C. Bright, MRS Bull. **25**, 15 (2000).
[2] H. Hosono, Int. J. Appl. Ceram. Technol. **1**, 106 (2004).
[3] T. Minami, MRS Bull. **25**, 38 (2000).
[4] B. G. Lewis and D. C. Paine, MRS Bull. **25**, 22 (2000).
[5] G. Thomas, Nature (London) **389**, 907 (1997).
[6] H. Bartl and T. Scheller, Neues Jahrb. Miner. Monatsh. **35**, 547 (1970).
[7] K. Hayashi, S. Matsuishi, T. Kamiya, M. Hirano, and H. Hosono, Nature (London) **419**, 462 (2002).
[8] K. Hayashi, P. V. Sushko, A. L. Shluger, M. Hirano, and H. Hosono, J. Phys. Chem. B **109**, 23836 (2005).
[9] S. Matsuishi, K. Hayashi, M. Hirano, and H. Hosono, J. Am. Chem. Soc. **127**, 12454 (2005).
[10] J. E. Medvedeva, A. J. Freeman, M. I. Bertoni, and T. O. Mason, Phys. Rev. Lett. **93**, 016408 (2004).
[11] J. E. Medvedeva and A. J. Freeman, Europhys. Lett. **69**, 583 (2005).
[12] M. I. Bertoni, T. O. Mason, J. E. Medvedeva, A. J. Freeman, K. R. Poeppelmeier, and B. Delley, J. Appl. Phys. **97**, 103713 (2005).
[13] S. Fujita, M. Ohkawa, K. Suzuki, H. Nakano, T. Mori, and H. Masuda, Chem. Mater. **15**, 4879 (2003).
[14] S. Fujita, K. Suzuki, M. Ohkawa, T. Mori, Y. Iida, Y. Miwa, H. Masuda, and S. Shimada, Chem. Mater. **15**, 255 (2003).
[15] F. Pertlik, Geolines **15**, 113 (2003).
[16] R. Siauciunas and A. Baltusnikas, Cem. Concr. Res. **33**, 1789 (2003).
[17] S. Matsuishi, Y. Toda, M. Miyakawa, K. Hayashi, T. Kamiya, M. Hirano, I. Tanaka, and H. Hosono, Science **301**, 626 (2003).
[18] M. Miyakawa, K. Hayashi, M. Hirano, Y. Toda, T. Kamiya, and H. Hosono, Adv. Mater. **15**, 1100 (2003).
[19] L. J. van der Pauw, Philips Res. Rep. **13**, 1 (1958).
[20] B. S. Hong, S. J. Ford, and T. O. Mason, Key Eng. Mater. **125**, 163 (1997).
[21] J. Hwang, Ph.D. thesis, Northwestern University, 1996.
[22] E. Wimmer, H. Krakauer, M. Weinert, and A. J. Freeman, Phys. Rev. B **24**, 864 (1981).
[23] O. K. Andersen and M. Jepsen, *Electronic Band Structure and Its Applications* (Springer, Berlin, 1986).
[24] J. E. Medvedeva and A. J. Freeman, Appl. Phys. Lett. **85**, 955 (2004).
[25] The fact that the conductivity has a hopping nature follows from the detailed analysis of the self-consistent density of states (DOS) of the UV-activated systems. We found that the largest contributions in the vicinity of E_F are from the particular atoms which are spatially well separated from each other. Furthermore, the DOS at E_F exhibits a Coulomb gap—a distinctive feature of variable range hopping. Fitting the Coulomb gap allowed predictions of the characteristic temperatures which agree well with experiment (see Ref. 10).
[26] N. M. Tallan, *Electrical Conductivity in Ceramics and Glass* (Marcel Dekker, New York, 1974).
[27] J. Nell, B. J. Wood, S. E. Dorris, and T. O. Mason, J. Solid State Chem. **82**, 247 (1989).
[28] D. P. Karim and A. T. Aldred, Phys. Rev. B **20**, 2255 (1979).
[29] T. O. Mason and H. K. Bowen, J. Am. Ceram. Soc. **64**, 237 (1981).
[30] E. Gartstein, T. O. Mason, and J. B. Cohen, Am. Ceram. Soc. Bull. **60**, 375 (1981).
[31] P. V. Sushko, A. L. Shluger, K. Hayashi, M. Hirano, and H. Hosono, Thin Solid Films **445**, 161 (2003).
[32] Z. Y. Li, J. L. Yang, J. G. Hou, and Q. S. Zhu, Angew. Chem., Int. Ed. **43**, 6479 (2004).